A systematic review and comparison of automated tools for quantification of fibrous networks

de Vries, Judith J.; Laan, Daphne M.; Frey, Felix; Koenderink, Gijsje H.; de Maat, Moniek P.M.

DOI
10.1016/j.actbio.2022.12.009

Publication date
2023

Document Version
Final published version

Published in
Acta Biomaterialia

Acta Biomaterialia 157 (2023) 263–274

Contents lists available at ScienceDirect

Acta Biomaterialia

journal homepage: www.elsevier.com/locate/actbio

Full length article

A systematic review and comparison of automated tools for quantification of fibrous networks☆

Judith J. de Vries[a], Daphne M. Laan[a], Felix Frey[b,c], Gijsje H. Koenderink[b], Moniek P.M. de Maat[a,*]

[a] Department of Hematology, Erasmus MC, University Medical Center Rotterdam, Rotterdam, The Netherlands
[b] Department of Bionanoscience, Kavli Institute of Nanoscience, Delft University of Technology, Delft, the Netherlands

ARTICLE INFO

Article history:
Received 23 September 2022
Revised 30 November 2022
Accepted 5 December 2022
Available online 10 December 2022

Keywords:
Fibrin
Fibrous networks
Image processing
Microscopy
Systematic review

ABSTRACT

Fibrous networks are essential structural components of biological and engineered materials. Accordingly, many approaches have been developed to quantify their structural properties, which define their material properties. However, a comprehensive overview and comparison of methods is lacking. Therefore, we systematically searched for automated tools quantifying network characteristics in confocal, stimulated emission depletion (STED) or scanning electron microscopy (SEM) images and compared these tools by applying them to fibrin, a prototypical fibrous network in thrombi. Structural properties of fibrin such as fiber diameter and alignment are clinically relevant, since they influence the risk of thrombosis. Based on a systematic comparison of the automated tools with each other, manual measurements, and simulated networks, we provide guidance to choose appropriate tools for fibrous network quantification depending on imaging modality and structural parameter. These tools are often able to reliably measure relative changes in network characteristics, but absolute numbers should be interpreted with care.

Statement of significance

Structural properties of fibrous networks define material properties of many biological and engineered materials. Many methods exist to automatically quantify structural properties, but an overview and comparison is lacking. In this work, we systematically searched for all publicly available automated analysis tools that can quantify structural properties of fibrous networks. Next, we compared them by applying them to microscopy images of fibrin networks. We also benchmarked the automated tools against manual measurements or synthetic images. As a result, we give advice on which automated analysis tools to use for specific structural properties. We anticipate that researchers from a large variety of fields, ranging from thrombosis and hemostasis to cancer research, and materials science, can benefit from our work.

1. Introduction

Fibrous networks are critical structural components of many biological and engineered materials and are therefore studied in a wide range of fields. In a biomedical context, important examples include collagen or elastin fibers found in the extracellular matrix of mammalian connective tissues [1,2], fibrin fibers found in thrombi [3], and neurons in the brain [4]. Material scientists widely use fibrous networks to engineer hydrogels [5], paper, and textiles [6]. The structural characteristics of fibrous networks, such as the fiber length, diameter, density and alignment, dictate the physical properties of these materials, including their elastic modulus, strength, and permeability [7]. A distinction can be made between fiber properties, describing characteristics of individual fibers such as diameter, and network properties, describing the network as a whole such as fiber density or alignment. The structure of fibrous networks is commonly determined by

☆ Authors confirm they have checked all supplementary files (removing any highlighting of the edits) and e-Extra content tabs.

* Corresponding author at: Department of Hematology, Erasmus MC, University Medical Center Rotterdam, P.O. Box 2040 3000CA Rotterdam, the Netherlands.
E-mail address: m.demaat@erasmusmc.nl (M.P.M. de Maat).
[c] Present address: Institute of Science and Technology, Klosterneuburg, Austria

https://doi.org/10.1016/j.actbio.2022.12.009

imaging, in particular by scanning electron microscopy (SEM) or confocal microscopy. SEM provides high resolution, but requires extensive sample preparation such as dehydration and sputter coating, which can affect network properties and introduce imaging artefacts [8]. Preparation of samples for confocal microscopy is less invasive, but this method has a limited resolution and can therefore not reliably measure the diameter of fibers, which are often below 200 nm in biological materials [9] and synthetic hydrogels [10]. Recently developed super-resolution methods such as stimulated emission depletion (STED) microscopy offer a good alternative, but are so far not exploited much for fibrous networks. STED microscopy selectively switches off fluorophores around the focal point, thereby increasing resolution below 50 nm and improving the differentiation of separate fibers [11]. An advantage of STED microscopy over other super-resolution techniques is that it is applicable to samples prepared in the same way as for confocal microscopy.

Many different approaches have been developed for the (semi-)automated quantification of fibrous network characteristics from microscopy images, though often in a specific and narrow context, such as collagen or (synthetic) nanofibers [12] and neurites in neurons [13]. It is unknown to what extent these tools can be used across fields for other types of fibrous networks. More generally, it is unclear which methods are suitable for which structural characteristics because a comprehensive overview is missing. Therefore, our first aim is to provide an overview of publicly available automated tools that can be used to quantify fibrous network characteristics. Next, we systematically tested these tools on confocal, STED, and SEM images of fibrin networks, a representative example of a biological fibrous network with high clinical relevance. Fibrin is the main structural component of the thrombus that forms upon blood clotting. Structural properties of fibrin are important determinants of the disease burden and mortality associated with various diseases, such as cardiovascular disease and inflammatory diseases such as COVID-19 [14–16]. The fibrin network forms after activation of the coagulation cascade, ultimately leading to the cleavage of fibrinogen molecules into fibrin monomers that laterally and longitudinally associate into thick fibers that form branched networks [17]. Characteristics of the fibrin network, such as fiber thickness, pore size, and number of branch points, determine among others the risk of embolization and the susceptibility of thrombi to fibrinolysis [18]. For instance, in patients with thrombotic disease, more compact thrombi are observed that are characterized by many thin fibers, a dense fibrin network with small pores, and a large number of branch points [19]. This results in decreased permeability for proteins of the fibrinolytic system, enhancing resistance to breakdown of the thrombus [20].

Here we systematically searched the literature for available automated tools that can be used to quantify characteristics of fibrous networks. By testing these tools on confocal, STED, and SEM images of fibrin networks in addition to testing them on synthetic and simulated images, we provide guidance to choose appropriate tools for the quantification of fibrous network characteristics.

2. Methods

The systematic review was performed according to the Preferred Reporting Items for Systematic Reviews and Meta-Analyses (PRISMA) guidelines [21].

2.1. Article search

We conducted a systematic literature search in the Embase, Medline-Ovid, Cochrane Library, and Web of Science databases on April 2nd, 2021; and the search was repeated on November 7, 2021 and May 10, 2022. The search strategy included different types of fibrous networks, such as fibrin, collagen, and nanofibers, in combination with image analysis terms (e.g. algorithm or automated analysis), different microscopes (e.g. fluorescence, confocal, scanning electron microscopy), and network characteristics (e.g. diameter, pore size, orientation, length). For the full search terms, see the Supplementary Information.

2.2. Study selection

After deduplication, the search resulted in 5799 results (Fig. 1). Two researchers (J.J. de Vries and D.M. Laan) independently screened these articles. In the first step, articles were included based on title and abstract. Subsequently, these abstracts were read full text and articles that did not match the research questions were excluded. Reasons for exclusions were: manual measurements, no quantification of (relevant) parameters, no (relevant) imaging, or when the paper was only theoretical. In addition, reviews and articles not available in full text were excluded. While reading the articles, additional relevant articles based on the bibliography were also assessed for inclusion. In case of disagreement between the two researchers, consensus was reached through discussion.

2.3. Data extraction

To prevent bias, data were independently extracted from the articles by two researchers (J.J. de Vries and D.M. Laan). The following data was collected: first author, publication year, name of the used tool, type of network the tool was used on, imaging modality used to make the images, and quantified characteristics (alignment, fiber diameter, fiber length, fiber density, number of branch points or junctions, pore size and/or porosity).

2.4. Testing and comparison of the automated tools

After identification of the automated tools, these tools were tested on different sets of images of fibrin networks to assess whether the tools worked on these images and resulted in automated quantification of relevant characteristics. Tools were excluded when manual steps such as manual tracing were needed, when only images from specific devices could be used, when the software was commercial, or when specific requirements were needed that were not present in our fibrin network images (e.g. multiple imaging channels or specific shapes, such as a neuron body). Next, tools that worked on our fibrin images were applied on a test set of fibrin network images and results of the different tools were compared. The test set of fibrin network images consisted of 50 scanning electron microscopy (SEM) images with a pixel size of 8.3 nm [9], 100 confocal laser scanning microscopy images (50 images of clots formed under static conditions with a pixel size of 67.6 nm [16,22], and 50 images of clots formed in a flow chamber at different shear rates with a pixel size of 94.6 nm), and 50 stimulated emission depletion (STED) microscopy images with a pixel size of 26.4 nm [16,22]. Further details on these images can be found in the Supplementary Methods and examples can be found in Fig. 2A. Before analyzing the images using the automated tools, STED and confocal images were preprocessed by subtracting the background. A rolling ball radius of 50 pixels for STED images and 25 pixels for confocal images was used. These settings were based on the size of the largest objects in the images. In addition, other relevant preprocessing steps were used when this was deemed necessary for a good performance of the analysis tool (Supplementary Table

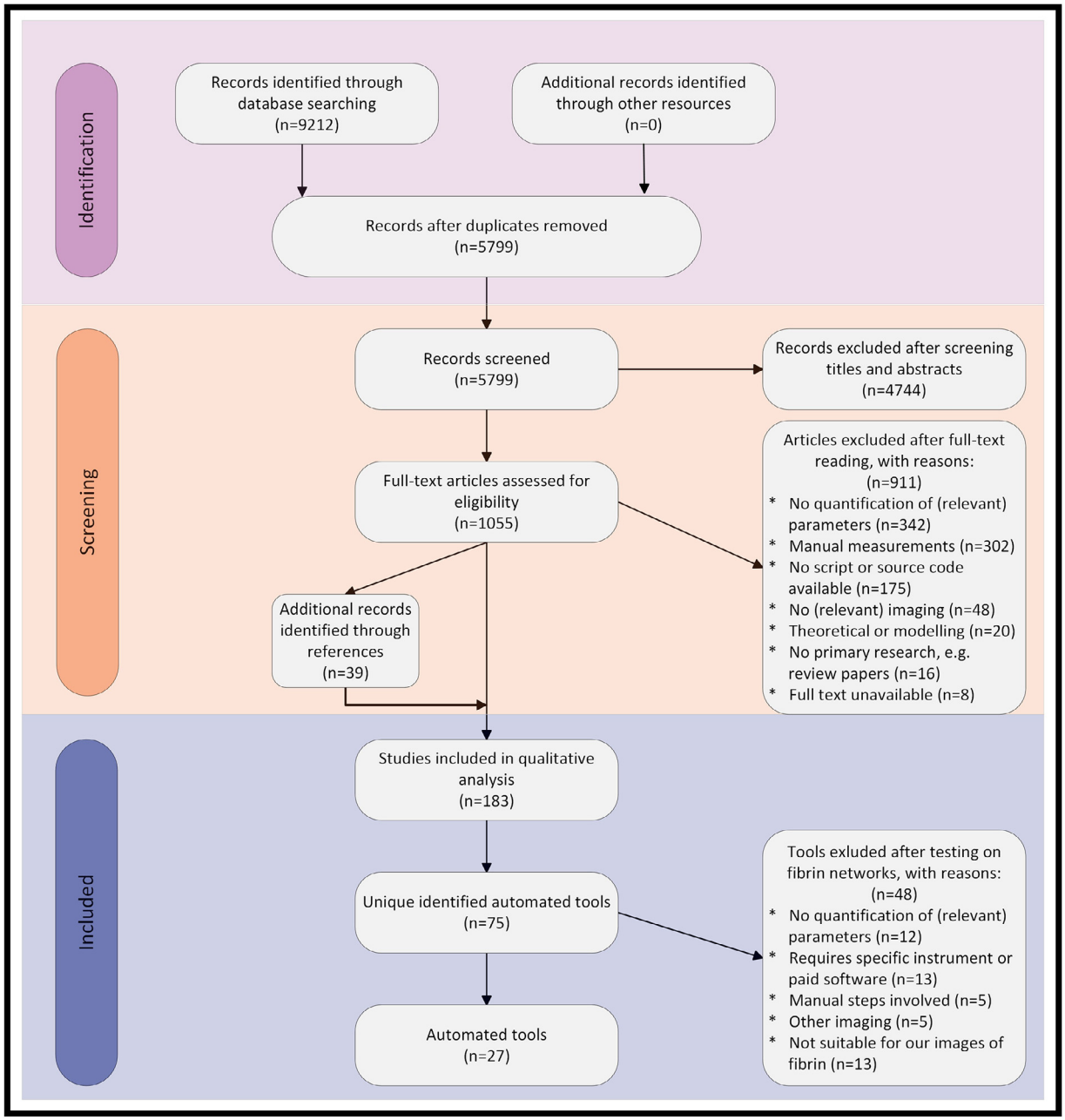

Fig. 1. PRISMA (Preferred Reporting Items for Systematic Reviews and Meta-Analyses [21]) flow diagram of study selection. In the identification phase, we systematically searched the literature to identify articles using automated tools that quantify fibrous network characteristics. In the screening phase, articles were first screened based on title and abstract. Next, articles were read full-text to assess their eligibility. Finally, we included 183 articles in which automated analysis tools were used, of which we extracted 75 different tools. We applied these tools to fibrin, a prototypical fibrous network example present in thrombi. Of the 75 tools, 27 could be used on our confocal, stimulated emission depletion (STED), or scanning electron microscopy (SEM) images. The results of these tools were compared to each other, manual measurements, and simulated networks.

XVIII). Most of the settings in each tool were left as their default settings, except when stated otherwise in Supplementary Table XVIII.

2.5. Comparing automated tools on synthetic images and simulated fibrous networks

To test the performance of each tool, we also applied the automated tools to digital synthetic images of branched fibrous networks with flexible fibers with known diameters, generated by Hotaling et al. [23]. We used 15 images with a monodisperse fiber diameter and nine images with polydispersity in the thickness of fibers (see Fig. 3B and C for examples). All tools able to measure diameter were applied to these images. Additionally, we used 13 synthetic images containing rigid, short fibers with known dispersion parameters ranging from 0.2 to 5, generated by Morrill et al. [24] (see Fig. 3A for examples). These images all had a mean fiber orientation of 90°. All tools able to measure fiber alignment were applied to these images.

Finally, we used three simulated branched fibrous networks with flexible fibers with known diameters, branch point number

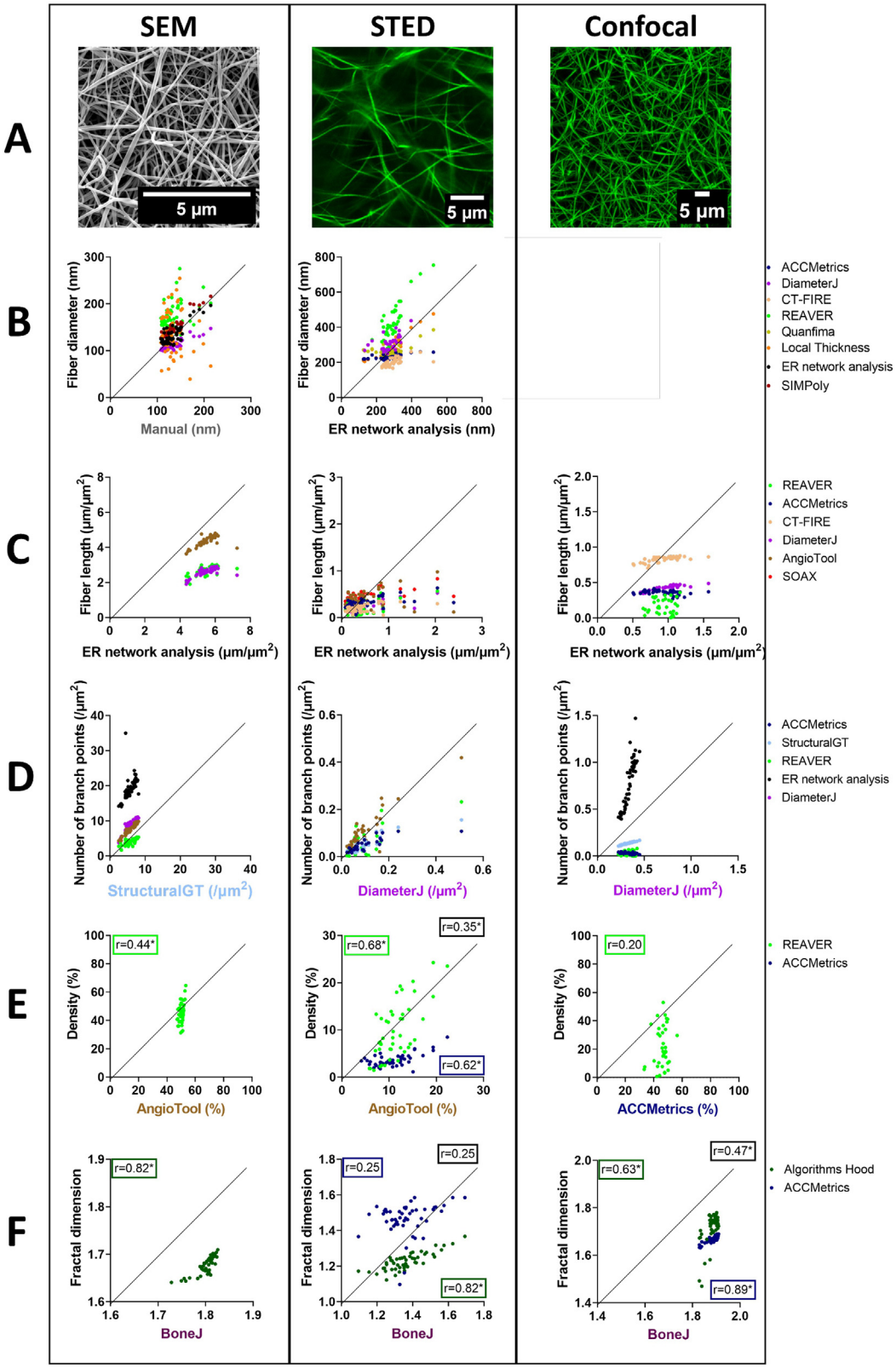

Fig. 2. Correlation between the results of the different tools applied to SEM, STED, and confocal images (A) to quantify fibrin fiber diameter (B), fiber length (C), number of branch points (D), fibrin network density (E), and fractal dimension (F). The solid lines in (B-F) indicate the x=y-lines. B) Manual measurements of fiber diameter were used as reference on the x-axis in the SEM images, while the fiber diameters quantified by the ER network analysis were used as reference in the STED images, since its absolute values were closest to the manual measurements in SEM. Every dot presents the mean fiber diameter per image. C) For fiber length measurements, the results of the ER network analysis were used as reference, since the results from this tool were closest to known values in synthetic images. Total fiber length measured by the different tools was divided by the surface area of the image, to be able to compare absolute values between different imaging methods. Every dot represents the fiber length per µm^2 in one image. D) For the quantification of the number of branch points, the numbers calculated by StructuralGT (SEM) and DiameterJ (STED and confocal) were used as reference, since these tools performed best on simulated networks with known number of branch points. The total number of branch points was divided by the surface area of the image. Therefore, every dot represents the number of branch points per µm^2 in one image. E, F) Fibrin network density and fractal dimension were quantified by only two or three tools. Therefore, Pearson's correlation coefficients (r) are given for every combination of tools in the graph, indicated by boxes in the color of the dots of the correlation of that specific tool with the tool on the x-axis, or in black boxes when two tools on the y-axis are correlated; *p<0.05.

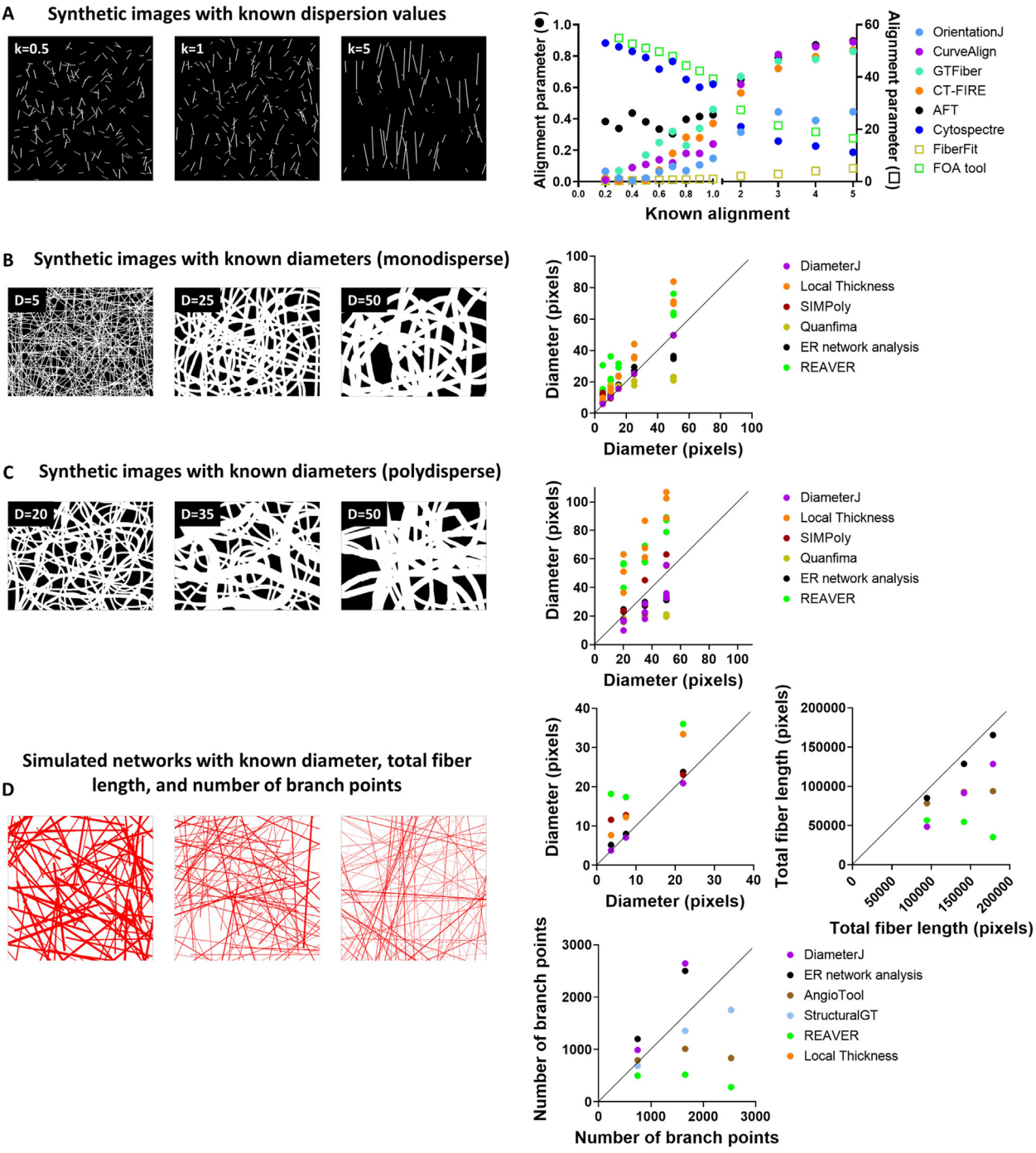

Fig. 3. Examples of (A) synthetic images with known dispersion (k) values [24], synthetic images with (B) monodisperse or (C) polydisperse diameters [23], and (D) simulated networks. Correlation plots show the known values on the x-axis and the results of the different tools on the y-axis. The solid lines indicate the x=y-lines. Every dot represents the result of one image. In B and C, three different images per diameter value were used, while in A and D, only one image per value was used.

and fiber length (Fig. 3D). The algorithm to generate fibrous networks was written in Python (See Supplementary Information) and more information is available in the Supplementary Methods.

2.6. Statistical analysis

For each quantified characteristic, we assessed the correlation between results obtained using the different tools, reporting the Pearson's correlation coefficient (r). All tools able to quantify a specific characteristic were used in the comparison of that characteristic.

2.7. Data availability

The full set of confocal, STED, SEM, and simulated images are available from the authors upon request. The numbers obtained after applying the automated tools on the images are available in a data supplement.

2.8. Code availability

The Python code to generate simulated images can be found in a data supplement available with the online version of this

Table 1
Overview of identified automated tools that can be used to quantify fibrin fiber network characteristics..

Name of the tool	Type of network it was developed for	Image type it was developed for	Confocal	SEM	STED	Batchprocessing	2D/3D	Reference
ACCMetrics	Nerve fibers	Confocal	√	✗	√	√	2D	[32,33]
DiameterJ	Nanofibers	SEM	✗	√	√	√	2D	[34]
CT-FIRE	Collagen	SHG	√	✗	√	√	2D/3D	[29]
FIRE (FIbeR Extraction)	Collagen	Confocal microscopy	√	✗	√	✗	2D/3D	[28]
Local Thickness plugin	In general, bone tissue as example	In general	√	√	√	√	2D	[35,36]
SIMPoly	Nanofibers	SEM	✗	√	✗	✗	2D	[37]
ER Network Analysis	Endoplasmic reticulum	Confocal microscopy	√	√	√	√	2D	[38]
REAVER	Vascular networks	High-resolution fluorescence microscopy	✗	√	√	√	2D	[39]
Quanfima	Fibrous biomaterials	In general	√	√	√	√	2D/3D	[40]
Qiber3D	Networks	3D image stacks	√	✗	✗	✗	3D	[30]
Algorithms Hood et al.	Fibrin	Confocal microscopy	√	√	√	√	2D	[41]
AngioTool	Vascular networks	Fluorescence microscopy	✗	√	√	✗	2D	[42]
SOAX	Biopolymer networks	Confocal microscopy	√	✗	√	√	2D/3D	[43]
StructuralGT	Nanoscale networks	SEM	✗	√	√	√	2D	[44]
BoneJ	Bone	Computed Tomography	√	√	√	√	2D/3D	[45]
Pore size analysis (Krauss et al.)	Collagen	Confocal microscopy	√	✗	✗	✗	2D	[46]
Hydrogel analysis	Hydrogels	Cryo-SEM	√	✗	✗	✗	2D	[47]
Bubble analysis	Biopolymer networks	Confocal	√	√	✗	√	2D	[48]
3D directional variance algorithm	Collagen	SHG	√	✗	√	✗	3D	[31]
CurveAlign	Collagen	SHG	√	√	√	√	2D/3D	[49]
OrientationJ	Collagen	Confocal	√	√	√	√	2D	[50]
Directionality plugin	-	-	√	√	√	✗	2D	None
FibLab/FOA tool	Fibrous networks	Fluorescence microscopy	√	√	√	✗	2D	[51]
Cytospectre	Cytoskeleton filaments	Microscopy images	√	√	√	√	2D	[52]
FiberFit	Collagen	Confocal microscopy	√	√	√	√	2D	[24]
GTFiber	Nanofibers	AFM	√	√	√	√	2D	[53]
AFT (Alignment by Fourier Transform)	Fibrillar features	Microscopy images	√	√	√	√	2D	[54]

article. The software and scripts of the used methods identified in the systematic search can be found via the original publications.

3. Results

3.1. Study selection

A total of 9212 articles was found in the literature search (see Supplementary Information for the full search terms). After deduplication, 5799 articles were screened based on title and abstract (Fig. 1). From the 1055 articles read in full text, we included 144 articles in which an automated tool was used that was publicly available as a script, program, or plugin. In addition, while reading these articles full text, we identified 39 other relevant articles that met the inclusion criteria in the references which were also included. In total, we identified 75 different automated tools or scripts in 183 papers.

3.2. Testing of the automated tools

The selected tools were tested on our confocal, STED, and SEM images of fibrin networks to check whether they can be used on fibrin networks imaged using one of these imaging techniques. From the 75 tools, 48 tools were excluded. Reasons for exclusion during testing were, among others, that some tools required manual processing steps, could only be used on images from specific devices, needed paid software, or were not suitable for our images of fibrin fibers (Supplementary Table I). This last category includes tools that for example looked for cross-sections of fibers [25], needed multi-channel images [26,27], or needed specific kinds of structures, such as cell bodies in neurons [13].

3.3. Comparison of the automated tools

Next, the automated tools that could be used on our fibrin network images were applied to 100 confocal (50 of fibrin networks formed under static conditions and 50 of fibrin networks formed under flow), 50 SEM, and 50 STED images of fibrin networks (see Supplementary Fig. I-IV for visual presentations of the applied tools). Many of the automated image analysis tools were originally developed for collagen or nanofibers (Table 1). Most tools were suitable for confocal, STED, and SEM images and could be used with a batch processing option. In addition, most tools quantified network characteristics in 2D, while some were able to also, or solely, use 3D image stacks. Most of the identified tools were able to quantify fibrin fiber diameter, fiber length, or alignment (Table 2). Three of the 27 tools were not included in the comparison analyses. FIRE [28] was not used, since CT-FIRE [29] was used instead, which is an extension of FIRE. Qiber3D [30] and the 3D directional variance algorithm [31] could only be used on 3D image stacks. However, all other tools were applied to 2D images, so we did not include Qiber3D and the 3D directional variance algorithm in the comparison analyses.

AFM, atomic force microscopy; SEM, scanning electron microscopy; SHG, second-harmonic generation; STED, stimulated emission depletion.

3.3.1. Fiber alignment

We tested nine tools that could quantify alignment, a characteristic describing the network as a whole (Supplementary Table II): OrientationJ [50], CurveAlign [49], GTFiber [53], CT-FIRE [29], Cytospectre [52], Directionality, FOA tool [51], FiberFit [24], and Alignment by Fourier Transform (AFT) [54]. Most of the methods measured global alignment (within the whole image), while OrientationJ, GTFiber, and AFT used local alignment measurements

Table 2
Overview of quantified characteristics per tool.

	Fiber properties			Network properties				
Image analysis tool	Fiber orientation	Fiber diameter	Fiber length	Alignment	Branch points	Fiber density	Fractal dimension	Porosity/Pore size
ACCMetrics	✗	√	√	✗	√	√	√	✗
DiameterJ	✗	√	√	✗	√	✗	✗	√
CT-FIRE	√	√	√	√	✗	✗	✗	✗
FIRE (FIbeR Extraction)	✗	✗	√	✗	√	√	✗	✗
Local Thickness plugin	✗	√	✗	✗	✗	✗	✗	✗
SIMPoly	✗	√	✗	✗	✗	✗	✗	✗
ER Network Analysis	✗	√	√	✗	√	✗	✗	✗
REAVER	✗	√	√	✗	√	√	✗	✗
Quanfima	√	√	✗	✗	✗	✗	✗	√
Qiber3D	✗	√	√	✗	√	√	✗	✗
Algorithms Hood et al.	✗	✗	✗	✗	✗	✗	√	√
AngioTool	✗	✗	√	✗	√	√	✗	✗
SOAX	√	✗	√	✗	✗	✗	✗	✗
StructuralGT	✗	✗	✗	✗	√	✗	✗	✗
BoneJ	✗	✗	✗	✗	✗	✗	√	✗
Pore size analysis (Krauss et al.)	✗	✗	✗	✗	✗	✗	✗	√
Hydrogel analysis	✗	✗	✗	✗	✗	✗	✗	√
Bubble analysis	✗	✗	✗	✗	✗	✗	✗	√
3D directional variance algorithm	✗	✗	✗	√	✗	✗	✗	✗
CurveAlign	√	✗	✗	√	✗	✗	✗	✗
OrientationJ	√	✗	✗	√	✗	✗	✗	✗
Directionality	√	✗	✗	√	✗	✗	✗	✗
FibLab/FOA tool	√	✗	✗	√	✗	✗	✗	✗
Cytospectre	√	✗	✗	√	✗	✗	✗	✗
FiberFit	√	✗	✗	√	✗	✗	✗	✗
GTFiber	✗	✗	✗	√	✗	✗	✗	✗
AFT (Alignment by Fourier Transform)	✗	✗	✗	√	✗	✗	✗	✗

(within the local neighborhood). To compare these tools, we applied them to confocal images of fibrin fibers aligned by applying shear flow with different shear rates. Visual examples of the applied tools are shown in Supplementary Fig. IV. Supplementary Fig. V shows the 50 images with their corresponding nematic order parameter (S) as calculated by OrientationJ. OrientationJ was used as reference because of its proven sensitivity for fiber alignment [55]. OrientationJ and the CurveAlign, GTFiber, CT-FIRE and AFT tools provide an orientation parameter that describes the alignment with a value between 0 (randomly aligned) and 1 (perfectly aligned). Strong correlations were found between these five tools, with good agreement in absolute levels between OrientationJ and CurveAlign and between CT-FIRE, GTFiber, and AFT (Supplementary Table II and Supplementary Fig. VI). CT-FIRE, GTFiber, and AFT report levels that are clearly higher than OrientationJ and CurveAlign. Cytospectre also returns a value between 0 and 1, but in this case the alignment parameter is defined such that 1 means randomly aligned and 0 means perfectly aligned. This is opposite to the other tools, which explains the negative correlations. FiberFit returns the fiber dispersion parameter, which is analogous to the reciprocal of variance in fiber orientation, therefore low values mean disordered networks and large values mean aligned networks. FiberFit shows a significant correlation with OrientationJ. Finally, the directionality plugin and the FOA tool result in parameters describing the spread of the orientation distribution. Lower values represent better aligned fibers, while higher values represent more variation and therefore less aligned fibers. Directionality and the FOA tool appear to be rather insensitive to alignment as quantified by OrientationJ.

Additionally, we applied the tools to synthetic images generated based on a semicircular von Mises probability density function [24] with known dispersion parameters (Fig. 3A and Supplementary Table III). Since all tools report different outcome parameters with different absolute values, we could not compare absolute values to the known dispersion parameter. Similar to the results in the confocal images, we did see very strong significant correlations ($r>0.85$) of the results of almost all tools with the known dispersion values, except for the FOA tool ($r=-0.73$, $p<0.05$). The Directionality plugin did not provide useful results from these images, since no reliable fit could be made to the histogram.

3.3.2. Fiber diameter

To quantify fibrin fiber diameter (a fiber property), we identified eight automated tools: DiameterJ [34], Local Thickness plugin [35,36], REAVER [39], ER network analysis [38], ACCMetrics [32,33], CT-FIRE [29], Quanfima [40] and SIMPoly [37]. Visual presentations of these algorithms can be found in Supplemental Figs. I and II. Because a high image resolution is needed to quantify fibrin fiber diameters, we only tested these tools on STED and SEM images (Fig. 2A). For SEM images, we benchmarked the results from the automated tools against manually measured fiber diameters [9]. Both in SEM and STED images, almost all tools showed strong correlations with each other (Fig. 2B and Supplementary Table IV and V). SIMPoly and the ER network analysis found similar absolute values as the manual measurements in SEM images. By contrast, DiameterJ systematically underestimated fiber thickness. The mean diameter measured by DiameterJ was 17% lower than the manual measurement. The Local Thickness plugin and REAVER showed no or weak correlations with the manual measurements, as well as a large overestimation (31%) of the fiber thickness in the case of REAVER. In the STED images, we used the results of the ER network analysis for reference since the mean value of the diameter calculated by this tool was closest to the manual measurement of the diameter in the SEM images. All other tools showed strong correlations with the ER network analysis tool and with each other in STED images. The absolute diameter values in STED images ranged from 200 nm (measured by CT-FIRE) to 400 nm (measured by REAVER).

To further check the performance of the tools, we next tested them also on synthetic images of fibrous networks drawn using the freehand tool in Inkscape [23] with either known and validated monodisperse fiber diameters between 5 and 50 pixels (Fig. 3B) or polydisperse fiber diameters with an average of 20, 35, or 50 pixels (Fig. 3C), and to simulated networks with known characteristics (Fig. 3D and Supplementary Fig. VII), generated using an algorithm in Python (see Supplementary Information for the Python code). We used both synthetic images of fibers that were published and validated previously for DiameterJ and FiberFit, as well as fibrous networks that we simulated ourselves to be able to perform unbiased comparisons. DiameterJ performed well in synthetic images and the simulated networks with constant fiber diameters, while diameter values were underestimated (on average by 44%) in the synthetic images with polydisperse fiber diameters (Supplementary Table VI). This limitation is a consequence of the intersection subtraction of DiameterJ. [34] Thicker fibers are more likely to have more intersections due to their increased size. Therefore, thicker fibers will have less influence on the mean diameter than thinner fibers, which results in an underestimation of the mean fiber diameter. Fibrin networks are usually polydisperse in terms of fiber diameters [56], making DiameterJ less suitable for absolute diameter quantification. The Local Thickness plugin and REAVER were sensitive to changes in fiber diameters in the synthetic images, but significantly overestimated (mean) fiber thickness by respectively 79% and 121%. SIMPoly performed well in images containing fibers with a thickness between 10 and 50 pixels, while the fiber thickness in the images with the thinnest fibers was not correctly measured. This is probably caused by an unsuccessful detection of the thinner fibers. The ER network analysis on the other hand showed correct values for fibers with a diameter up to 25 pixels, while fibers of 50 pixels were underestimated. Visual inspection showed that in very thick fibers, sometimes two centerlines were drawn, which might explain this underestimation. Quanfima was rather insensitive to changes in fiber diameter. Overall, we recommend to use ER network analysis or SIMPoly to measure fibrin fiber diameters.

3.3.3. Fiber length

We found seven different tools that quantify fiber length (a fiber property) in confocal, STED, or SEM images: DiameterJ [34], AngioTool [42], REAVER [39], ER network analysis [38], CT-FIRE [29], ACCMetrics [32,33], and SOAX [43] (Fig. 2C). Visual presentations of these algorithms can be found in Supplemental Figs. I, II, and III. The results of these tools showed strong correlations with each other when applied to STED and SEM images, but not for confocal images (Supplementary Tables VII-IX). Absolute values of fiber length, normalized against the surface area of the image, were higher in SEM images compared to STED and confocal images, likely since SEM images show fibers from multiple layers whereas STED and confocal show fibers only within the confocal slice. Applying the automated tools to simulated networks showed that the ER network analysis returned values very similar to the known values (Fig. 3D and Supplementary Table X). DiameterJ was sensitive to changes, but underestimated fiber length, while AngioTool and REAVER were not sensitive to fiber length. We hence recommend to use the ER network analysis to automatically determine fiber length.

3.3.4. Number of branch points

To automatically quantify the number of branch points (a network property), we found six tools: DiameterJ [34], AngioTool [42], StructuralGT [44], REAVER [39], ER network analysis [38], and ACCMetrics [32,33] (see Supplementary Figs. I, II, and III for visual presentations of these algorithms). Again, strong correlations were found between the results of the tools in both SEM and STED images, with remarkably higher absolute numbers of branch points per μm^2 in SEM than in STED or confocal images (Fig. 2D and Supplementary Tables XI-XIII). In confocal images, significant associations were present between DiameterJ, StructuralGT, and the ER network analysis. However, absolute numbers of the different tools showed a very broad range, suggesting that confocal imaging is not a reliable tool for measuring branch points. In SEM images, REAVER reported a significantly lower number of branch points compared to the majority of tools, while the ER network analysis resulted in a significantly higher number. In STED images, also a large range of numbers was found: between 30 (StructuralGT and ACCMetrics) and 70 (DiameterJ and AngioTool). Upon inspection of the fiber tracing results, we observed that StructuralGT and ACCMetrics did not detect all fibers and therefore all branch points present in STED images, while DiameterJ and AngioTool performed better (Supplementary Fig. III). When analyzing the simulated networks, we observed the best results for StructuralGT (Fig. 3D and Supplementary Table XIV). DiameterJ and the ER network analysis overestimated the number of branch points, while AngioTool and REAVER were insensitive to changes in the number of branch points. Based on visual inspection and the results from the simulated images, we recommend to use StructuralGT in SEM images and DiameterJ in STED images to automatically measure the number of branch points.

3.3.5. Fiber density

We found three different tools to quantify the density of the fibrin network (a network property): AngioTool [42], REAVER [39], and ACCMetrics [32,33]. Density is defined as the fraction or percentage of the area occupied by fibers. Similar to the branching analysis, significant correlations were observed between the quantifications in SEM and STED images, while results in confocal images did not significantly correlate (Fig. 2E). Absolute numbers strongly varied between different automated tools with no tool clearly being most reliable (Supplementary Table XV).

3.3.6. Fractal dimension

Fractal dimension can be used to investigate complexity of the network. It measures how details in an object change with the scale at which it is measured [57]. BoneJ [45], algorithms developed by Hood et al. [41], and ACCMetrics [32,33] were able to analyse the fractal dimension in our fibrin networks. In SEM and STED images, a strong correlation between the fractal dimension calculated by BoneJ and Algorithms of Hood et al. was found, while ACCMetrics gave different results in STED images (Fig. 2F and Supplementary Table XVI). In confocal images, the three tools correlated strongly.

3.3.7. Pore size and porosity

Finally, we found some tools that automatically measured pore size or porosity (network properties). Pore size is defined as the mean size of the pores in the fibrous network, and porosity is the fraction of the area occupied by pores. In SEM images, we could only use DiameterJ [34] and the Bubble analysis tool [48] to measure mean pore size. DiameterJ reports mean pore area in μm^2, while the Bubble analysis tool reports the mean pore diameter in µm. No correlation between both measurements was found ($r=-0.12$, $p=0.40$) (Supplementary Fig. VIIIA). In confocal images, six different tools were found which report pore size, pore diameter, or porosity: DiameterJ [34] (mean pore area and porosity), Pore size analysis by Krauss et al. [46] (mean pore diameter), Bubble analysis [48] (mean pore diameter), Hydrogel pore size analysis [47] (mean pore area, mean pore diameter, and porosity), Algorithms by Hood et al. [41] (porosity), and Quanfima [40] (porosity) (Supplementary Table XVII and Supplementary Fig. VIIIB-C). Except for the Hydrogel analysis, the porosity measurements correlated quite well between the different tools. Pore size measure-

ments by the different tools showed only significant correlations when the same parameter was calculated, either diameter or pore area. The pore diameters measured by the Pore size analysis by Krauss et al. [46] and the Bubble analysis [48] did also not correlate with the porosity measurements, while the tools calculating pore area [34,47] did show significant correlations with the porosity measurements. Visual presentations of these algorithms can be found in Supplemental Figs. I and III.

4. Discussion

We systematically searched the literature for all available tools that automatically quantify structural characteristics of fibrous networks from either electron or light microscopy images. Next, we compared the results from the identified automated tools when applied to confocal, STED, and SEM images of fibrin networks, a prototypical fiber with biological and clinical relevance. We found 27 different automated tools that were publicly available and could be applied to our images. Of these tools, a minority were originally developed for fibrin (Table 1). This shows the importance of making research tools available and findable across different fields.

Using the identified tools, we measured the fiber properties fiber diameter and fiber length, and the network properties alignment, number of branch points, fiber density, fractal dimension, pore size, and porosity. It was striking that the results of the different automated tools often showed good correlations, while the absolute numbers varied a lot. This suggests that most tools are able to measure relative changes in fibrous network characteristics but absolute numbers should be interpreted with care. Therefore, we recommend that comparison of fibrous network characteristics should always be performed using the same type of microscopy image and analysis tool. A possible explanation for differences between algorithms is the fact that some tools were developed for imaging techniques other than confocal, STED, or SEM, which might result in a mismatch in image size or resolution when the tool is applied to another technique than it was originally developed for. Another observation we made is that the correlations between results from different automated tools were often stronger in the images with high resolution (SEM and STED) than in the confocal images. For confocal images, the optical diffraction limit, being comparable to the size of the fibers, probably limits the reliability of automated analysis of fiber and junction features. Moreover, out of focus light might also influence the measurements. However, confocal images may be preferred in measurements of fiber alignment, network density and fractal dimension because of their larger field of view compared to electron microscopy and the possibility of 3D reconstruction from Z-stacks. Furthermore, absolute numbers of fiber length per μm^2, number of branch points per μm^2, and density were higher in SEM than in STED and confocal images. This is likely caused by the fact that the scanning electron microscope images the surface of fibrous networks and captures fibers from multiple layers, whereas STED and confocal microscopy optically filter out fibers from above and below the confocal plane. The smaller fiber diameter in SEM than in STED images can probably be explained by shrinkage of the clot in SEM due to the preparation, or some remaining out of focus light in STED images. We acknowledge that in addition to confocal, STED, and SEM microscopy, also other imaging techniques are being used for studying fiber networks, such as AFM [58] and multiphoton microscopy [59]. We decided to not include those type of images in our comparisons, since these techniques are currently less commonly used than confocal and SEM imaging. Finally, our systematic search revealed that many articles use automated ways of measuring fibrous network characteristics, without making their tools or scripts available. Therefore, to increase standardization and transparency, open access of newly developed tools should be promoted.

Most of the publicly available automated tools in this study were developed for the characterization of fiber or network characteristics in 2D images. While 2D imaging and quantification is often easier and takes less computing time, it should be noted that measurements in 3D might result in more accurate estimations of these characteristics. 2D images do not contain information about the third dimension of the structures, and results from these images might be different when taken from different angles. Nowadays, imaging and automated tools that are able to quantify characteristics in 3D are increasingly being developed, which should lead to a broader availability of these tools. Because we only identified a very limited number of publicly available tools that are able to quantify fiber and network characteristics in 3D [30,31,43], we decided to focus our comparative analyses on the 2D characterization. Future studies are therefore needed to systematically apply and compare automated tools for 3D fibrous networks when sufficient publicly available tools are available.

Most of the identified tools were developed for the quantification of fiber alignment, fiber diameter or fiber length of fibrous networks. Alignment of fibers in fibrous networks affects cellular behavior, such as cell attachment, migration, and differentiation, which is important in tissue engineered scaffolds [60], wound healing, and - in case of fibrin - the susceptibility of thrombi to fibrinolysis [61,62]. We tested nine different tools to automatically quantify alignment of fibrin fibers. These tools either resulted in a nematic order parameter between 0 and 1 or a parameter quantifying the spread of the orientation distribution. In general, the different tools showed good correlations, showing that most tools can be reliably used to measure fibrin fiber alignment in confocal images. Using synthetic images with known fiber dispersion confirmed that most of the tools, except for the Directionality plugin, performed well in the quantification of fiber alignment. We recommend a tool that returns a nematic order parameter, since this provides a sensitive measure between 0 and 1 that can be linked directly to theoretical models that connect fiber alignment to mechanical properties [55,63]. When also taking into account the ease of use of the tools and the possibility to adapt parameters, our preferences to quantify fiber alignment in fibrin networks go towards OrientationJ [50,64] (ImageJ plugin), CurveAlign [49] (MATLAB-based standalone application), or FiberFit [24] (Python-based standalone application).

Until recently, quantification of fiber diameters was often done manually, which is inefficient and sensitive to observer bias [9,65]. We tested eight available tools to automatically measure fiber diameter. Our analyses showed that both in SEM and STED images, fiber diameter quantifications were strongly correlated among different methods, while absolute values differed markedly. Using manual measurements and synthetic and simulated images, we showed that SIMPoly and the ER network analysis tools reported values closest to the true diameters. Therefore, we recommend to use SIMPoly in SEM images and the ER network analysis in SEM or STED images. However, both tools showed some variation in performance based on the width and polydispersity of the fibers. The optimal thickness of fibers in images is between 10 and 25 pixels for both tools, which would require a pixel size between 10 and 25 nm for typical fibrin fibers. SIMPoly is a MATLAB-based tool that is very user-friendly [37]. The ER network analysis tool provides more user control because it has many options that can be adjusted, but it therefore requires more testing by the user for their specific images [38].

Fiber length, the number of branch points, and fiber density are other characteristics which are often used to describe the organization of fibrous networks. Increased branching is associated with thinner fibers, which is characteristic for more dense fibrin net-

Table 3
Overview of fibrous network characteristics with their appropriate imaging technique and recommended tool for automated analysis.

Structural characteristic	Imaging technique			Automated tool
	Confocal	STED	SEM	
Fiber alignment	√	✗	✗	OrientationJ FiberFit CurveAlign
Fiber diameter	✗	√	√	ER network analysis SIMPoly
Fiber length	✗	√	√	ER network analysis
Branch points	✗	√	√	DiameterJ StructuralGT
Fiber density	✗	√	√	-
Fractal dimension	√	✗	✗	-
Pore size/porosity	√	✗	✗	-

works [66]. Our analyses showed that in SEM and STED, good correlations were found between the different tools. For fiber length, best results were obtained with the ER network analysis, while StructuralGT gave the best results in the quantification of the number of branch points. Our results indicate that electron microscopy is more suited than confocal imaging for precise quantification of fiber length and the number of branch points. For fiber density, absolute numbers strongly varied between the three different automated tools with no tool clearly being most reliable.

The fractal dimension of fibrin networks is known to increase with increasing thrombin concentration and a denser fibrin network structure [67–69]. Moreover, a recent study suggests that fractal dimension of the fibrin network is a biomarker for a high risk of venous thrombosis [69]. In our analysis, we found only three tools that measured fractal dimension, with variable results. More research should be performed to determine whether this characteristic can be reliably measured in microscopy images to describe network complexity of fibrous networks, for example by comparing it to fractal dimension quantifications using rheology [70].

Finally, pore size and porosity were quantified by six different tools. When measuring pore size, only moderate correlations were found between the results from the different tools. In contrast, porosity measurements of different tools were more strongly correlated. Correlations between pore size and porosity measurements were best when the pore area was calculated instead of the pore diameter, suggesting a circle might not be the best description of a pore. A major drawback of the included tools is the fact that the pores are mostly measured in 2D images, while it is important to measure pores in 3D to get reliable information since pores can have different sizes in all three dimensions. Pore size and porosity as measured by DiameterJ were indeed shown to be poorly correlated with functional permeability measurements of plasma clots [9]. While pore sizes have been measured in 3D [71–73], and it was shown that it is possible to work with 2D images while correcting for the missing third dimension [74], these tools are unfortunately not publicly available. We conclude that automated tools exist that can measure porosity and/or pore size in 2D images, preferably by measuring pore area, but that better tools should become publicly available.

5. Conclusions

In conclusion, we have made an overview of a large number of automated quantification tools for fibrous networks and systematically compared them on fibrin networks, a prototypical example of a fibrous network in thrombi (Table 3). We conclude that fiber diameter can be measured reliably and efficiently by SIMPoly or the ER network analysis in SEM or STED images. For fiber alignment, we recommend using OrientationJ, CurveAlign, or FiberFit on confocal images. Fiber length can be measured using the ER network analysis, while we recommend DiameterJ or StructuralGT to measure the number of branch points in SEM or STED images. For the other network characteristics, such as fractal dimension or pore size, more development and open access publication of automated tools is needed. We anticipate that our analysis provides researchers useful guidelines in their search for suitable automated analysis tools of fibrous networks in different fields, from thrombosis and hemostasis to cancer research, regenerative medicine, materials science, and neuroscience.

Funding

F.F. gratefully acknowledges funding from the Kavli Synergy program of the Kavli Institute of Nanoscience Delft. G.H.K. gratefully acknowledges funding from the NWO Talent Programme which is financed by the Dutch Research Council (NWO) (project number VI.C.182.004). The sponsors had no involvement in the study design, collection, analysis and interpretation of data, or in the writing of the report and the decision to submit the article for publication.

Declaration of Competing Interest

The authors declare no competing financial interests.

CRediT authorship contribution statement

Judith J. de Vries: Conceptualization, Methodology, Investigation, Formal analysis, Visualization, Writing – original draft. **Daphne M. Laan:** Investigation, Formal analysis, Visualization, Writing – review & editing. **Felix Frey:** Software, Writing – review & editing. **Gijsje H. Koenderink:** Writing – review & editing, Supervision. **Moniek P.M. de Maat:** Conceptualization, Writing – review & editing, Supervision.

Acknowledgements

The authors wish to thank Wichor M. Bramer from the Erasmus MC Medical Library for developing and updating the search strategies, Marieke J.H.A. Kruip and Caroline S.B. Veen for providing us with the SEM images and manual measurements of the fiber diameters, Emmelien D. Hazekamp for her help with some of the MATLAB tools, and Trevor J. Lujan for providing us with test images with known dispersions.

Supplementary materials

Supplementary material associated with this article can be found, in the online version, at doi:10.1016/j.actbio.2022.12.009.

References

[1] C. Frantz, K.M. Stewart, V.M. Weaver, The extracellular matrix at a glance, J. Cell Sci. 123 (Pt 24) (2010) 4195–4200.
[2] H. Vindin, S.M. Mithieux, A.S. Weiss, Elastin architecture, Matrix Biol. 84 (2019) 4–16.
[3] M.W. Mosesson, Fibrinogen and fibrin structure and functions, J. Thromb. Haemost. 3 (8) (2005) 1894–1904.
[4] S.Y. Ho, C.Y. Chao, H.L. Huang, T.W. Chiu, P. Charoenkwan, E. Hwang, NeurphologyJ: an automatic neuronal morphology quantification method and its application in pharmacological discovery, BMC Bioinformatics 12 (2011) 230.
[5] E.M. Ahmed, Hydrogel: Preparation, characterization, and applications: a review, J. Adv. Res. 6 (2) (2015) 105–121.
[6] R.C. Picu, Mechanics of random fiber networks—a review, Soft Matter. 7 (15) (2011) 6768–6785.
[7] F. Burla, Y. Mulla, B.E. Vos, A. Aufderhorst-Roberts, G.H. Koenderink, From mechanical resilience to active material properties in biopolymer networks, Nat. Rev. Phys. 1 (4) (2019) 249–263.
[8] S.E. Kirk, J.N. Skepper, A.M. Donald, Application of environmental scanning electron microscopy to determine biological surface structure, J. Microsc. 233 (2) (2009) 205–224.
[9] A. Daraei, M. Pieters, S.R. Baker, Z. de Lange-Loots, A. Siniarski, R.I. Litvinov, C.S.B. Veen, M.P.M. de Maat, J.W. Weisel, R.A.S. Ariens, M. Guthold, Automated Fiber Diameter and porosity measurements of plasma clots in scanning electron microscopy images, Biomolecules 11 (10) (2021) 1536.
[10] P.H. Kouwer, M. Koepf, V.A. Le Sage, M. Jaspers, A.M. van Buul, Z.H. Eksteen-Akeroyd, T. Woltinge, E. Schwartz, H.J. Kitto, R. Hoogenboom, S.J. Picken, R.J. Nolte, E. Mendes, A.E. Rowan, Responsive biomimetic networks from polyisocyanopeptide hydrogels, Nature 493 (7434) (2013) 651–655.
[11] S.W. Hell, J. Wichmann, Breaking the diffraction resolution limit by stimulated emission: stimulated-emission-depletion fluorescence microscopy, Opt. Lett. 19 (11) (1994) 780–782.
[12] S. Stojanov, A. Berlec, Electrospun nanofibers as carriers of microorganisms, stem cells, proteins, and nucleic acids in therapeutic and other applications, Front. Bioeng. Biotechnol. 8 (2020) 130.
[13] S.Y. Ho, C.Y. Chao, H.L. Huang, T.W. Chiu, P. Charoenkwan, E. Hwang, NeurphologyJ: an automatic neuronal morphology quantification method and its application in pharmacological discovery, BMC Bioinformatics 12 (2011).
[14] K.I. Bridge, H. Philippou, R. Ariens, Clot properties and cardiovascular disease, Thromb. Haemost. 112 (5) (2014) 901–908.
[15] S. Dauwerse, H. Ten Cate, H.M.H. Spronk, M. Nagy, The composition and physical properties of clots in COVID-19 pathology, Diagnostics 12 (3) (2022).
[16] J.J. de Vries, C. Visser, L. Geers, J.A. Slotman, N.D. van Kleef, C. Maas, H.I. Bax, J.R. Miedema, E.C.M. van Gorp, M. Goeijenbier, J.P.C. van den Akker, H. Endeman, D.C. Rijken, M. Kruip, M.P.M. de Maat, Altered fibrin network structure and fibrinolysis in intensive care unit patients with COVID-19, not entirely explaining the increased risk of thrombosis, J. Thromb. Haemost. 20 (6) (2022) 1412–1420.
[17] J.W. Weisel, R.I. Litvinov, Fibrin formation, structure and properties, Subcell. Biochem. 82 (2017) 405–456.
[18] A. Undas, Fibrin clot properties and their modulation in thrombotic disorders, Thromb. Haemost. 112 (1) (2014) 32–42.
[19] A. Undas, R.A. Ariens, Fibrin clot structure and function: a role in the pathophysiology of arterial and venous thromboembolic diseases, Arterioscler. Thromb. Vasc. Biol. 31 (12) (2011) e88–e99.
[20] J.P. Collet, D. Park, C. Lesty, J. Soria, C. Soria, G. Montalescot, J.W. Weisel, Influence of fibrin network conformation and fibrin fiber diameter on fibrinolysis speed: dynamic and structural approaches by confocal microscopy, Arterioscler. Thromb. Vasc. Biol. 20 (5) (2000) 1354–1361.
[21] D. Moher, A. Liberati, J. Tetzlaff, D.G. Altman, P. Group, Preferred reporting items for systematic reviews and meta-analyses: the PRISMA statement, J. Clin. Epidemiol. 62 (10) (2009) 1006–1012.
[22] M.P. de Maat, M. van Schie, C. Kluft, F.W. Leebeek, P. Meijer, Biological variation of hemostasis variables in thrombosis and bleeding: consequences for performance specifications, Clin. Chem. 62 (12) (2016) 1639–1646.
[23] N.A. Hotaling, K. Bharti, H. Kriel, C.G. Simon Jr., Dataset for the validation and use of DiameterJ an open source nanofiber diameter measurement tool, Data Brief 5 (2015) 13–22.
[24] E.E. Morrill, A.N. Tulepbergenov, C.J. Stender, R. Lamichhane, R.J. Brown, T.J. Lujan, A validated software application to measure fiber organization in soft tissue, Biomech. Model. Mechanobiol. 15 (6) (2016) 1467–1478.
[25] C.R. Stevens, J. Berenson, M. Sledziona, T.P. Moore, L. Dong, J. Cheetham, Approach for semi-automated measurement of fiber diameter in murine and canine skeletal muscle, PLoS One 15 (12) (2020) e0243163.
[26] Y. Zong, I. Pruner, A. Antovic, A. Taxiarchis, Z.P. Vila, N. Soutari, F. Mobarrez, R. Chaireti, J. Widengren, J. Piguet, J.P. Antovic, Phosphatidylserine positive microparticles improve hemostasis in in-vitro hemophilia A plasma models, Sci. Rep. 10 (1) (2020) 7871.
[27] A.C. Canver, A. Morss Clyne, Quantification of multicellular organization, junction integrity, and substrate features in collective cell migration, Microsc. Microanal. 23 (1) (2017) 22–33.
[28] A.M. Stein, D.A. Vader, L.M. Jawerth, D.A. Weitz, L.M. Sander, An algorithm for extracting the network geometry of three-dimensional collagen gels, J. Microsc. 232 (3) (2008) 463–475.
[29] J.S. Bredfeldt, Y.M. Liu, C.A. Pehlke, M.W. Conklin, J.M. Szulczewski, D.R. Inman, P.J. Keely, R.D. Nowak, T.R. Mackie, K.W. Eliceiri, Computational segmentation of collagen fibers from second-harmonic generation images of breast cancer, J. Biomed. Opt. 19 (1) (2014).
[30] A. Jaeschke, H. Eckert, L.J. Bray, Qiber3D - An open-source software package for the quantitative analysis of networks from 3D image stacks, GigaScience 11 (2022).
[31] Z. Liu, L. Speroni, K.P. Quinn, C. Alonzo, D. Pouli, Y. Zhang, E. Stuntz, C. Sonnenschein, A.M. Soto, I. Georgakoudi, 3D organizational mapping of collagen fibers elucidates matrix remodeling in a hormone-sensitive 3D breast tissue model, Biomaterials 179 (2018) 96–108.
[32] M.A. Dabbah, J. Graham, I. Petropoulos, M. Tavakoli, R.A. Malik, Dual-model automatic detection of nerve-fibres in corneal confocal microscopy images, Int. Conf. Med. Image Comput. Comput.-Assisted Intervent. 13 (Pt 1) (2010) 300–307.
[33] X. Chen, J. Graham, M.A. Dabbah, I.N. Petropoulos, M. Tavakoli, R.A. Malik, An automatic tool for quantification of nerve fibers in corneal confocal microscopy images, IEEE Trans. Biomed. Eng. 64 (4) (2017) 786–794.
[34] N.A. Hotaling, K. Bharti, H. Kriel, C.G. Simon, DiameterJ: a validated open source nanofiber diameter measurement tool, Biomaterials 61 (2015) 327–338.
[35] T. Hildebrand, P. Ruegsegger, Quantification of bone microarchitecture with the structure model index, Comput. Methods Biomech. Biomed. Eng. 1 (1) (1997) 15–23.
[36] D. Dougherty, K. Kunzelmann, Computing local thickness of 3D structure with ImageJ, Micros Microanal. 13 (2007) 1678–1679.
[37] R. Murphy, A. Turcott, L. Banuelos, E. Dowey, B. Goodwin, K.O. Cardinal, SIMPoly: a matlab-based image analysis tool to measure electrospun polymer scaffold fiber diameter, Tissue Eng. Part C 26 (12) (2020) 628–636.
[38] M. Fricker, L. Heaton, N. Jones, B. Obara, S.J. Müller, A.J. Meyer, Quantitation of ER structure and function, Methods Mol. Biol. (2018) 43–66.
[39] B.A. Corliss, R.W. Doty, C. Mathews, P.A. Yates, T. Zhang, S.M. Peirce, REAVER: a program for improved analysis of high-resolution vascular network images, Microcirculation 27 (5) (2020) e12618.
[40] R. Shkarin, A. Shkarin, S. Shkarina, A. Cecilia, R.A. Surmenev, M.A. Surmeneva, V. Weinhardt, T. Baumbach, R. Mikut, Quanfima: an open source Python package for automated fiber analysis of biomaterials, PLoS One 14 (4) (2019).
[41] J.E. Hood, S. Yesudasan, R.D. Averett, Glucose concentration affects fibrin clot structure and morphology as evidenced by fluorescence imaging and molecular simulations, Clin. Appl. Thromb. Hemost. 24 (9_suppl) (2018) 104S–116S.
[42] E. Zudaire, L. Gambardella, C. Kurcz, S. Vermeren, A computational tool for quantitative analysis of vascular networks, PLoS One 6 (11) (2011).
[43] T. Xu, D. Vavylonis, F.C. Tsai, G.H. Koenderink, W. Nie, E. Yusuf, I.J. Lee, J.Q. Wu, X. Huang, SOAX: a software for quantification of 3D biopolymer networks, Sci. Rep. 5 (2015) 9081.
[44] D.A. Vecchio, S.H. Mahler, M.D. Hammig, N.A. Kotov, Structural analysis of nanoscale network materials using graph theory, ACS Nano 15 (8) (2021) 12847–12859.
[45] M. Doube, M.M. Kłosowski, I. Arganda-Carreras, F.P. Cordelières, R.P. Dougherty, J.S. Jackson, B. Schmid, J.R. Hutchinson, S.J. Shefelbine, BoneJ: Free and extensible bone image analysis in ImageJ, Bone 47 (6) (2010) 1076–1079.
[46] P. Krauss, C. Metzner, J. Lange, N. Lang, B. Fabry, Parameter-free binarization and skeletonization of fiber networks from confocal image stacks, PLoS One 7 (5) (2012).
[47] M. Jamshidi, C. Falamaki, Image analysis method for heterogeneity and porosity characterization of biomimetic hydrogels, F1000Res 9 (2020) 1461.
[48] S. Münster, B. Fabry, A simplified implementation of the bubble analysis of biopolymer network pores, Biophys. J. 104 (12) (2013) 2774–2775.
[49] Y. Liu, A. Keikhosravi, G.S. Mehta, C.R. Drifka, K.W. Eliceiri, Methods for quantifying fibrillar collagen alignment, Methods Mol. Biol. (2017) 429–451.
[50] R. Rezakhaniha, A. Agianniotis, J.T. Schrauwen, A. Griffa, D. Sage, C.V. Bouten, F.N. van de Vosse, M. Unser, N. Stergiopulos, Experimental investigation of collagen waviness and orientation in the arterial adventitia using confocal laser scanning microscopy, Biomech. Model. Mechanobiol. 11 (3-4) (2012) 461–473.
[51] E.E. van Haaften, T.B. Wissing, M.C.M. Rutten, J.A. Bulsink, K. Gashi, M.A.J. van Kelle, A. Smits, C.V.C. Bouten, N.A. Kurniawan, Decoupling the effect of shear stress and stretch on tissue growth and remodeling in a vascular graft, Tissue Eng. Part C 24 (7) (2018) 418–429.
[52] K. Kartasalo, R.-P. Pölönen, M. Ojala, J. Rasku, J. Lekkala, K. Aalto-Setälä, P. Kallio, CytoSpectre: a tool for spectral analysis of oriented structures on cellular and subcellular levels, BMC Bioinformatics 16 (1) (2015) 344.
[53] N.E. Persson, M.A. McBride, M.A. Grover, E. Reichmanis, Automated analysis of orientational order in images of fibrillar materials, Chem. Mater. 29 (1) (2017) 3–14.
[54] S. Marcotti, D.B. de Freitas, L.D. Troughton, F.N. Kenny, T.J. Shaw, B.M. Stramer, P.W. Oakes, A workflow for rapid unbiased quantification of fibrillar feature alignment in biological images, Front. Comput. Sci. 3 (2021).
[55] B.E. Vos, C. Martinez-Torres, F. Burla, J.W. Weisel, G.H. Koenderink, Revealing the molecular origins of fibrin's elastomeric properties by in situ X-ray scattering, Acta Biomater. 104 (2020) 39–52.
[56] G.A. Shah, I.A. Ferguson, T.Z. Dhall, D.P. Dhall, Polydispersion in the diameter of fibers in fibrin networks: consequences on the measurement of mass-length ratio by permeability and turbidity, Biopolymers 21 (6) (1982) 1037–1047.
[57] S.S. Cross, Fractals in pathology, J. Pathol. 182 (1) (1997) 1–8.
[58] R.G. Creasey, C.T. Gibson, N.H. Voelcker, Characterization of fiber-forming peptides and proteins by means of atomic force microscopy, Curr. Protein Pept. Sci. 13 (3) (2012) 232–257.

[59] G. Borile, D. Sandrin, A. Filippi, K.I. Anderson, F. Romanato, Label-free multiphoton microscopy: much more than fancy images, Int. J. Mol. Sci. 22 (5) (2021).
[60] S. Wang, S. Zhong, C.T. Lim, H. Nie, Effects of fiber alignment on stem cells-fibrous scaffold interactions, J. Mater. Chem. B 3 (16) (2015) 3358–3366.
[61] N. Laurens, P. Koolwijk, M.P. de Maat, Fibrin structure and wound healing, J. Thromb. Haemost. 4 (5) (2006) 932–939.
[62] R.A. Campbell, M. Aleman, L.D. Gray, M.R. Falvo, A.S. Wolberg, Flow profoundly influences fibrin network structure: implications for fibrin formation and clot stability in haemostasis, Thromb. Haemost. 104 (6) (2010) 1281–1284.
[63] V. Tutwiler, F. Maksudov, R.I. Litvinov, J.W. Weisel, V. Barsegov, Strength and deformability of fibrin clots: biomechanics, thermodynamics, and mechanisms of rupture, Acta Biomater. 131 (2021) 355–369.
[64] J. Alvarado, B.M. Mulder, G.H. Koenderink, Alignment of nematic and bundled semiflexible polymers in cell-sized confinement, Soft Matter. 10 (14) (2014) 2354–2364.
[65] G. Narayanan, M.Y. Tekbudak, Y. Caydamli, J. Dong, W.E. Krause, Accuracy of electrospun fiber diameters: the importance of sampling and person-to-person variation, Polym. Testing 61 (2017) 240–248.
[66] E.A. Ryan, L.F. Mockros, J.W. Weisel, L. Lorand, Structural origins of fibrin clot rheology, Biophys. J. 77 (5) (1999) 2813–2826.
[67] K. Hawkins, N. Badiei, J. Weisel, I. Chernysh, P.R. Williams, M.J. Lawrence, P.A. Evans, Fractal dimension: a biomarker for detecting acute thromboembolic disease, Critic. Care 16 (1) (2012) P431.
[68] M.J. Lawrence, A. Sabra, P. Thomas, D.R. Obaid, L.A. D'Silva, R.H. Morris, K. Hawkins, M.R. Brown, P.R. Williams, S.J. Davidson, A.J. Chase, D. Smith, P.A. Evans, Fractal dimension: a novel clot microstructure biomarker use in ST elevation myocardial infarction patients, Atherosclerosis 240 (2) (2015) 402–407.
[69] N.A. Davies, N.K. Harrison, R.H. Morris, S. Noble, M.J. Lawrence, L.A. D'Silva, L. Broome, M.R. Brown, K.M. Hawkins, P.R. Williams, S. Davidson, P.A. Evans, Fractal dimension (df) as a new structural biomarker of clot microstructure in different stages of lung cancer, Thromb. Haemost. 114 (6) (2015) 1251–1259.
[70] F. Bossler, J. Maurath, K. Dyhr, N. Willenbacher, E. Koos, Fractal approaches to characterize the structure of capillary suspensions using rheology and confocal microscopy, J. Rheol. 62 (1) (2018) 183–196.
[71] T. Fischer, A. Hayn, C.T. Mierke, Fast and reliable advanced two-step pore-size analysis of biomimetic 3D extracellular matrix scaffolds, Sci. Rep. 9 (1) (2019) 8352.
[72] K. Nakamura, T. Suda, K. Matsumoto, Characterization of pore size distribution of non-woven fibrous filter by inscribed sphere within 3D filter model, Separ. Purif. Technol. 197 (2018) 289–294.
[73] S.In Hwan, C. Young Jun, P.Chang Kyu, Automatic volumetric measurement of nanofiber webs using metaball approximation based on scanning electron microscope images, Textile Res. J. 80 (11) (2009) 995–1003.
[74] N.R. Lang, S. Munster, C. Metzner, P. Krauss, S. Schurmann, J. Lange, K.E. Aifantis, O. Friedrich, B. Fabry, Estimating the 3D pore size distribution of biopolymer networks from directionally biased data, Biophys. J. 105 (9) (2013) 1967–1975.